SUMMARY OF PROFESSIONAL ACHIEVEMENTS

THE DESIGN, COMPUTER SIMULATIONS AND FABRICATION OF OPTICAL METAMATERIALS

JAKUB HABERKO, PH. D.

AGH UNIVERSITY OF SCIENCE AND TECHNOLOGY

FACULTY OF PHYSICS AND APPLIED COMPUTER SCIENCE

KRAKÓW, 30TH NOVEMBER 2017

I would like to thank Professor Wojciech Łużny for his constant support and guidance since the time of my studies, a person without whom this work would not be possible.

I very warmly thank Professor Andrzej Bernasik for the intense and fruitful collaboration over the years.

Last but not least, I thank my Wife Justyna for her patience and encouragement.

1. Personal data

Name and surname

Jakub Haberko

Current employment

AGH University of Science and Technology

Faculty of Physics and Applied Computer Science

al. A. Mickiewicza 30

30-059 Kraków

POLAND

Phone number

(+48 12) 617 41 58

E-mail

haberko@fis.agh.edu.pl

2. Diplomas and scientific degrees with the name, awarding institution, year and thesis title

14.06.2004 – Master in technical physics

AGH University of Science and Technology

Faculty of Physics and Nuclear Techniques

Master thesis title: "Badania cienkowarstwowych kompozytów polimerowych" ("The study of thin film polymer composites")

Thesis supervisor: Prof. Wojciech Łużny

15.12.2008 – Ph. D. in physics

AGH University of Science and Technology

Faculty of Physics and Applied Computer Science

Ph.D. thesis title: "Separacja faz w cienkich warstwach kompozytów polianiliny" ("Phase separation in thin films of polyaniline composites")

Thesis supervisor: Prof. Wojciech Łużny

3. Employment in scientific institutions

01.12.2006 – 13.02.2009: assistant at the Faculty of Physics and Applied Computer Science, AGH University of Science and Technology in Krakow, Poland

from 14.02.2009: assistant professor at the Faculty of Physics and Applied Computer Science, AGH University of Science and Technology in Krakow, Poland

15.11.2010 – 01.11.2012: post-doc (*assistant-docteur*) in the Department of Physics, Faculty of Sciences, Fribourg University, Switzerland. At that time I was on a scientific leave from my home institution (AGH-UST).

4. *Scientific achievement, following the law on scientific degrees*

As a scientific achievement, being the base of the current application, I present a series of articles on a common topic (**[O1]**–**[O9]**).

4.1. Title of the achievement

The design, computer simulations and fabrication of optical metamaterials

4.2. Authors, titles of publications, publication year, publisher

[O1] **Jakub Haberko**, Frank Scheffold, *Fabrication of mesoscale polymeric templates for three-dimensional disordered photonic materials*, Optics Express 21 (1), 1057–1065 (2013).

IF(2013) = 3,525

My contribution to this work consisted in performing all the experiments and numerical calculations, writing the initial version of the manuscript, collaborating with the co-author on data interpretation and the final version of the paper.

I estimate my contribution at 80 %.

[O2] **Jakub Haberko**, Nicolas Muller, Frank Scheffold, *Direct laser writing of three-dimensional network structures as templates for disordered photonic materials*, Physical Review A 88 (4) 043822-1–043822-9 (2013).

IF(2013) = 2,991

My contribution to this work consisted in performing all the experiments and numerical calculations, writing the initial version of the manuscript, collaborating with the co-authors on data interpretation and the final version of the paper.

I estimate my contribution at 70 %.

[O3] Nicolas Muller, **Jakub Haberko**, Catherine Marichy, Frank Scheffold, *Silicon hyperuniform disordered photonic materials with a pronounced gap in the shortwave infrared*, Advanced Optical Materials 2 (2), 115–119 (2014).

IF(2014) = 4,062

My contribution to this work consisted in performing most DLW experiments, collaborating on the initial version of the CVD infiltration setup as well as collaborating on the final version of the manuscript.

I estimate my contribution at 30 %.

[O4] Nicolas Muller, **Jakub Haberko**, Catherine Marichy, Frank Scheffold, *Photonic hyperuniform networks obtained by silicon double inversion of polymer templates*, Optica 4 (3), 361–366 (2017).

IF(2016) = 7,727*

*The impact factor for 2017 is not yet available. Therefore the 2016 value is given here.

My contribution to this work consisted in programming the DLW instrument, performing a considerable portion of DLW experiments, designing and running the FDTD simulations and, in collaboration with other co-authors, analysing the data and preparing the final version of the manuscript.

I estimate my contribution at 20 %.

[O5] Luis S. Froufe-Pérez, Michael Engel, Pablo F. Damasceno, Nicolas Muller, **Jakub Haberko**, Sharon C. Glotzer, Frank Scheffold, *Role of Short-Range Order and Hyperuniformity in the Formation of Band Gaps in Disordered Photonic Materials*, Physical Review Letters 117, 053902-1–053902-5 (2016).

IF(2016)=8,462

My contribution to this work consisted in providing complementary 3D simulations necessary for the data interpretation.

I estimate my contribution at 10 %.

[O6] Maciej Kowalczyk, **Jakub Haberko**, Piotr Wasylczyk, *Microstructured gradient-index antireflective coating fabricated on a fiber tip with direct laser writing*, Optics Express 22 (10), 12545–12550 (2014).

IF(2014) = 3,488

My contribution to this work consisted in determining the effective refractive index profile and describing these calculations in the text, as well as in the collaboration with other co-authors on the manuscript.

I estimate my contribution at 40 %.

[O7] Łukasz Zinkiewicz, **Jakub Haberko**, Piotr Wasylczyk, *Highly asymmetric near infrared light transmission in an all-dielectric grating-on-mirror photonic structure*, Optics Express 23 (4), 4206–4211 (2015).

IF(2015) = 3,148

My contribution to this work consisted in simulating light propagation through the metamaterial and analyzing the simulation results. I have also prepared part of the scripts needed to program the DLW instrument. Moreover, I have described my simulations in the manuscript and collaborated with other co-authors on its final version.

I estimate my contribution at 45 %.

[O8] Łukasz Zinkiewicz, Michał Nawrot, **Jakub Haberko**, Piotr Wasylczyk, *Polarization-independent asymmetric light transmission in all-dielectric photonic structures*, Optical Materials 73, 484–488 (2017).

IF(2016) = 2,238*

*The impact factor for 2017 is not yet available. Therefore the 2016 value is given here.

My contribution to this work consisted in simulating light propagation through the metamaterial, analyzing simulation results and describing them in the text. I have also collaborated with other co-authors on the final version of the manuscript.

I estimate my contribution at 45 %.

[O9] **Jakub Haberko**, Piotr Wasylczyk, *Reflecting metallic metasurfaces designed with stochastic optimization as waveplates for manipulating light polarization*, Optics Communications 410 (2018) 740–743

IF(2016) = 1,588*

* The impact factor for 2018 and 2017 are not yet available. Therefore the 2016 value is given here.

My contribution to this work consisted in performing all computer simulations and calculations, preparing the figures and writing sections 2–4 of the manuscript.

I estimate my contribution at 90 %.

4.3. Description of the aim of the articles listed above and the results obtained as well as their possible application

4.3.1. Introduction

The term "optical metamaterials" [Cai] corresponds to artificially fabricated materials presenting non-typical optical properties or ones that are very difficult to achieve in ordinary materials. Their main characteristic is the fact that they are built of elements smaller than the wavelength at which they are supposed to operate. These elements, sometimes called meta-atoms, can, but do not have to, be periodically distributed inside the metamaterial. From the point of view of an incoming wave the metamaterial behaves as a uniform medium.

In this presentation, which constitutes a short summary of my research in this field initiated after obtaining the PhD degree and spanning the period of several years, I will describe the results of experiments and computer simulations which led to functional metamaterials meeting the desired specifications.

4.3.2. Non-periodic dielectric networks with a photonic band-gap

4.3.2.1. Photonic band-gap – from crystals to isotropic systems

In photonic crystals the electric permittivity changes periodically. In case of semiconductors such periodicity (but of the potential in which electrons are travelling) leads to the energy gap, that is a region of energies forbidden for an electron. Yablonovitch and John [Yabl, John] proved that a similar

effect may emerge for an electromagnetic wave in dielectrics with periodically varying dielectric constant. If the structure is chosen correctly and the refractive index contrast is high enough, light falling into the forbidden region cannot pass through the structure and it is reflected instead – a photonic band-gap (PBG) opens. It turns out, however, that strict periodicity in two or three dimensions is actually not a prerequisite for the PBG to appear. For instance quasicrystals, which are ordered systems but without the discrete translational symmetry, may also exhibit photonics band-gaps [Flor].

Crystals as well as quasicrystals are characterised by inherent anisotropy. It manifests itself in a different position of the photonic band-gap on the energy scale and its different width, depending on the angle of incidence of the incoming electromagnetic wave. If a PBG material didn't possess any long-range order, one could expect an anisotropic photonic band-gap. There are potentially numerous applications of such materials, from coloured dye-free coatings with no iridescence, through colour displays to optical waveguides and perfectly isotropic optical resonators. Following the path towards structures with smaller degree of order one can ask if long-range order is at all necessary for a photonic band-gap to open. Florescu et al. [Flor2] suggested that three conditions are sufficient: the structure should be hyperuniform, is should possess uniform local topology and short-range order.

The authors of [Flor] call a point pattern hyperuniform if its structure factor tends to zero for short wave vectors:

$$S(q) \xrightarrow[q \to 0]{} 0 \qquad (1)$$

This condition is equivalent to a statement that long-wavelength density fluctuations in such point pattern vanish. One can also express it in terms of the variance of the number of points $\left\langle N_R{}^2 \right\rangle - \left\langle N_R \right\rangle^2$ in a spherical window of size *R*. In a hyperuniform point pattern it grows more slowly than the size of the window $\sim R^d$, where *d* is the space dimension. All crystals and quasicrystals are hyperuniform. However, it turns out that there also exist point patterns without any long-range order which possess this property. A good example are geometrical centres of a random close packing (RCP) of monodisperse spheres. The authors give a recipe to generate an isotropic network with a PBG from a hyperuniform point pattern. The first step is to perform the Delaunay triangulation on the point pattern (Fig. 1a, blue points), which results in a set of triangles (Fig. 1a, blue lines). Next, geometrical centres of these triangles are calculated (Fig. 1a, red points) and dielectric cylinders are placed in these points (with axes perpendicular to the picture plane) and neighbouring points are connected with dielectric walls (their cross-sections with the picture plane are marked with red lines in Fig. 1a). This procedure leads to uniform local topology, since exactly three walls meet inside each cylinder. Numerical calculations show that such structure can possess an isotropic PBG, provided that the refractive index of the dielectric is high enough and the geometrical parameters of the structure, such as cylinder radius and wall thickness, are selected correctly. Further theoretical studies [Liew] allowed to expand this idea to three dimensions. The procedure of constructing a network form a point pattern is similar here, with the exception that the triangulation leads to a set of tetrahedra (instead of triangles), whose centres are connected with dielectric rods of finite thickness. Also in this case the local topology is uniform – in each vertex point exactly four dielectric rods meet.

Before the article **[O1]**, being part of a scientific achievement presented here, was published the PBG was only observed in 2-dimensional networks manufactured according to the recipe described above and for one polarization only. The PBG centre was in the microwave range (~20 GHz). The possibility of manufacturing 3-dimensinal structures operating in the infrared range is very interesting from the point of view of their potential applications in optics and telecommunication. One can imagine

using such structures as isotropic filters reflecting a selected wavelength range or for guiding light along a desired pathway in a three-dimensional structure. The aim of paper **[O1]**, which I based on my research, was to show that manufacturing such network structures with a characteristic length scale in the micron range was possible.

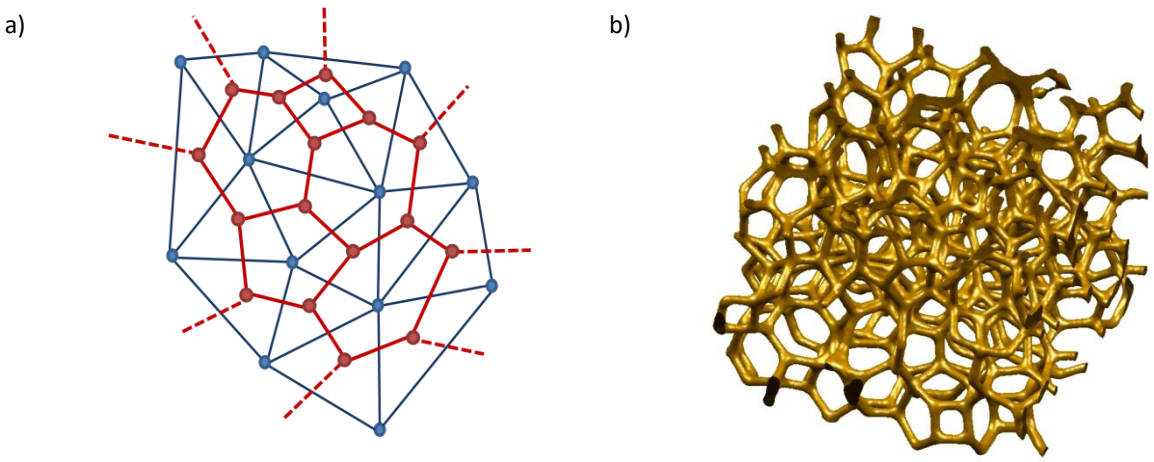

Fig. 1: a) From a hyperuniform point pattern in 2D to a 2D network with a photonic band-gap. ● – initial point pattern, —— – results of the Delaunay triangulation, ● – dielectric cylinders, —— – dielectric walls. b) A computer-generated image of a three-dimensional network based on a hyperuniform point pattern.

4.3.2.2. 3D printing for optical metamaterials – two-photon laser nanolithography

There exist several variants of the 3D printing method. Most of them work by adding material in a layer-by-layer fashion. However, it is impossible to reach sub-micron resolution on this route. In contrast the two-photon laser nanolithography (also termed direct laser writing, DLW) is capable of such precision. In this technique a liquid or gel-like polymer photoresist is illuminated with a pulsed femtosecond infrared laser light, which is focused through a high numerical aperture objective. In the focal spot the power in an impulse is sufficiently high for the two-photon absorption to take place, which leads to local photo-polymerisation of the resist. Polymerisation along the pathway of the laser (far from the focus) is avoided, since away from the focal spot the probability for the two-photon absorption is extremely low. This leads to high resolution of the manufactured structures. The glass slide with a droplet of the photoresist is placed on a piezoelectric table, whose position with respect to the focal point may be adjusted with nanometre precision. One can thus trace an almost arbitrary 3-dimensional polymerised path inside the sample. Following that the sample is placed in an organic solvent bath, which removes the non-illuminated photoresist, leaving a mechanically stable polymer structure. The spatial resolution in this method is equal to approximately 1 µm along the laser beam and around 0.3 µm in the perpendicular direction. This asymmetry is due to the point spread function of the objective. In other words the shape of the lithographic "pen" (or a lithographic voxel), with which one can write 3D structures is a prolate ellipsoid, elongated in the laser beam direction. This is also the shape of constant intensity surfaces around the focal point. By increasing the laser power one can adjust the volume of the ellipsoid, but this does not influence the aspect ratio of the lithographic voxel, which remains almost constant. In my studies I was using the Photonic Professional DLW apparatus by Nanoscribe and three different photoresists. As preliminary experiments for my research concerning disordered networks, which is described in this section, I fabricated other microstructures, for example the so-called woodpile photonic crystals (Fig. 2a), colloidal particles with various complicated shapes (Fig. 2b) and polymer microwires (Fig. 2c).

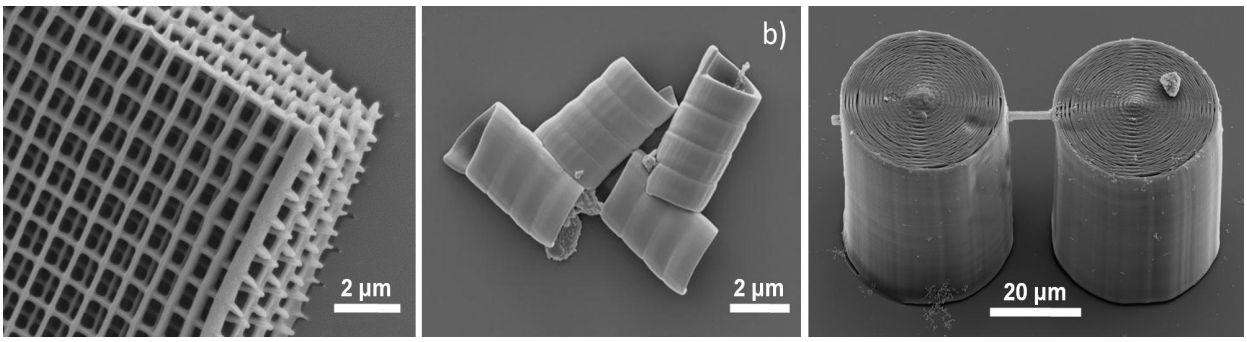

Fig. 2: Scanning electron micrographs of polymer structures fabricated by the author of the present Summary via the two-photon laser nanolithography. a) A woodpile photonic crystal. b) Helicoidal colloidal particles. c) A polymer microwire, used for electrical conductivity measurements after carbonization.

4.3.2.3. Fabrication and characterization of polymer hyperuniform networks

Because of the mechanical properties of the non-crosslinked photoresist, printing disordered 3D networks is more complicated than fabricating periodic structures. In the case of the woodpile structure, the photoresist is polymerized line by line and each consecutive one already at the moment of its creation is connected to the substrate or a previously written line, which renders the structure mechanically stable. However, such method would be impossible for a network similar to that in Fig. 1b. If a newly written rod is not within seconds connected with another element of the structure, the fluctuations in the liquid photoresist resulting from non-uniform temperature distribution inside the sample and the table movements may lead to a displacement of the rod and, as a consequence, the disruption of the structure. Furthermore, when preparing such a complicated structure one should avoid rapid movements of the piezoelectric scanner over long distances. Because of the scanner creep and hysteresis (issues known from atomic force microscopy) such movements inevitably lead to imprecise positioning of the lithographic "pen", which may have catastrophic consequences for the geometry of the fabricated structure. In order to overcome these problems I introduced a writing protocol, in which the sample is divided into cubic sections. Neighbouring sections are filled with dielectric rods, starting with those closest to the substrate. As a result one obtains a stable polymer network. Another difficulty lies in finding the corrects laser power. so that on the one hand each rod is thick enough to support the mechanical stability of the network and on the other hand to avoid overexposure of the network.

My research resulted in the creation of polymer networks with required geometry. Scanning electron micrographs show high overall quality of these structures (Fig. 3a). In order to enhance the mechanical stability the network was additionally surrounded by a 10 µm thick wall.

As mentioned above, the opening of a PBG requires a sufficiently high refractive index of the dielectric material. Like most polymers, the photoresist utilised here does not possess this property – it's refractive index is equal to merely n = 1.52. For this reason it is impossible to assess the quality of the material using spectroscopic methods. Hence in order to evaluate the average geometry of the networks I have performed measurements with a self-constructed visible light diffractometer. In this instrument red light from a He-Ne laser (λ = 632.8 nm) is focused on the network under study and the diffracted pattern is photographed off a white screen with a digital camera.

a) b)

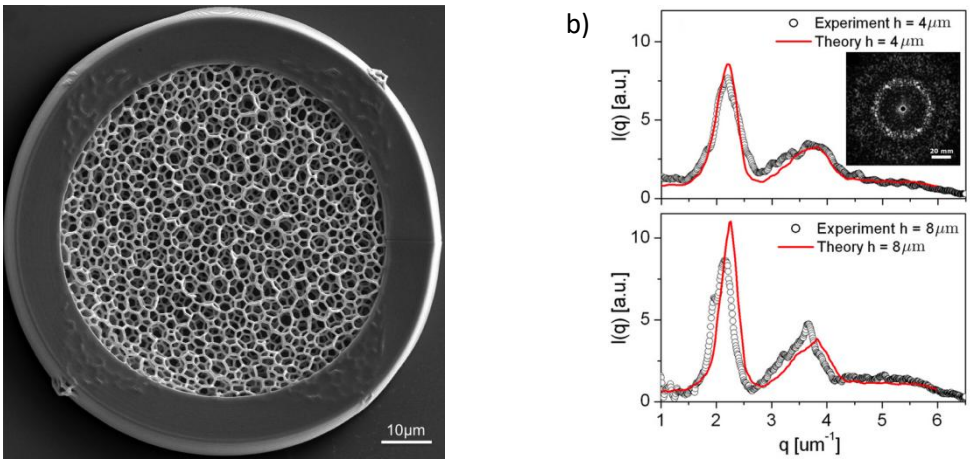

Fig. 3: a) Scanning electron micrograph of a 3D polymer network derived from a hyperuniform point pattern. b) Visible light diffraction measurements – diffraction pattern (inset) and its radial average for a network 4 µm high (upper panel) and 8 µm high (lower panel) and its comparison with theoretical results.

Initially the diffraction measurements were unsuccessful owing to multiple scattering of light on the polymer–air interface inside the network. It was therefore necessary to place the sample in an index-matching liquid, a mixture of organic solvents (toluene/chlorobenzene, $n = 1{,}517$). The diffraction pattern (Fig. 3b, inset) has a rotational symmetry, which reflects the network's isotropy. Furthermore, a speckle pattern characteristic of disordered systems is visible. However, the most prominent feature of the image is a ring of high diffracted intensity, resulting from the short-range order in the system. The value of the scattering vector corresponding to the ring (as well as each point on the screen) can be determined from the equations:

$$q = \frac{4\pi}{\lambda}\sin(\theta/2) \tag{2}$$

$$\tan(\theta) = u/z \tag{3}$$

where λ – wavelength in air, ϑ – scattering angle, u – distance of the ring form the screen centre, z – sample–screen distance. The maximum in the radially averaged pattern (Fig. 3b) corresponds to $q = 2.1\ \mu m^{-1}$, which translates to the distance $a = 2\pi/q \approx 3.0$ µm in real space, a value approximately equal to the sphere diameter in the initial hyperuniform point pattern (based on RCP).

The scattered light intensity as a function of the wave vector q can be calculated numerically. To this end I prepared a computer model of the studied structure, in which I assigned the value "1" to the vertices of the discrete grid lying inside the photoresist and "0" to the ones outside (that is in the air). In the single scattering approximation the scattered intensity is proportional to the squared modulus of the Fourier transform of the structure:

$$I(\vec{q}) \propto \left| \int f(\vec{r}) \exp(i\vec{q}\vec{r}) d\vec{r} \right|^2 \tag{4}$$

where *f(r)* is the above-mentioned binary representation of the network. This approached allowed me to calculate the expected scattered intensity for an arbitrary scattering vector. The comparison of the measured and calculated scattered intensity is shown in Fig. 3b. The agreement is excellent in the case of low networks ($h = 4$ µm) and good in the case of higher ones ($h = 8$ µm). The fact that the measured maxima are slightly lower than the calculated ones can be explained by a contribution of multiple

scattering in the experiment and networks' imperfections, which may be created at each fabrication step. Nevertheless, basing on the diffraction experiments and SEM measurements one can claim that in the course of these works high quality 3D networks with designed geometry were indeed manufactured

The article **[O2]** brought a considerable progress in the fabrication and studies of 3-dimensional hyperuniform networks. SEM photographs in Fig. 4a show high quality of the samples. The micrographs taken after focused ion beam (FIB) milling of the samples (Fig. 4b) attest to the fact that not only at the surface, but also deep inside the sample the designed geometry is retained and the structure is not overexposed. The elongation of dielectric rods in the direction perpendicular to the sample surface (along the laser beam), which was discussed before, is well visible here.

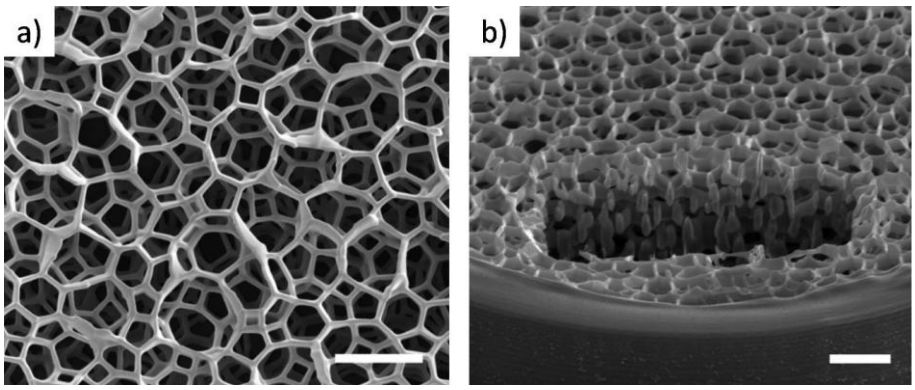

Fig. 4: a) Scanning electron micrograph of a 3D hyperuniform polymer network b) SEM micrograph after focused ion neam milling (FIB). Structure height: 16 µm. Bar length: 5 µm.

What is important, I was able to reduce the characteristic length scale of the structure by a factor 5/3 with respect to those presented in **[O1]** without the loss of quality. Fig. 5a shows a diffraction pattern of networks with a reduced length scale (a = 2 µm, the same sample–screen distance and q range as in Fig. 3b). The isotropic ring of high scattered intensity is still visible, but its distance from the image centre is higher than in Fig. 3b, which correspond to shorter distances in the direct space. The maximum of the radially averaged diffraction pattern clearly shifts towards longer wavevectors with decreasing the characteristic length scale of the structure (Fig. 5b).

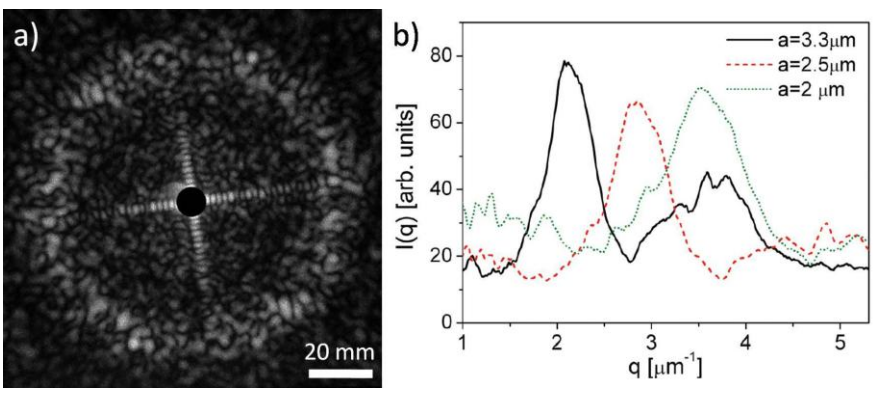

Fig. 5: a) Visible light diffraction on a structure with a characteristic length scale a = 2 µm. b) Towards smaller networks. Radially averaged scattered light intensity measured for networks with decreasing a value.

A numerical analysis of light scattering similar to that described above (Fig. 6c) demonstrates that the maximum of the diffraction peak increases with the structure height h and stabilizes at around h = 20 µm. This is important as far as observing a PBG in networks with higher refractive index is concerned. Since the photonic band-gap is linked to light scattering, one can expect that the full gap

may be observed only for relatively high structures. The scattered intensity at short wavevectors ($I(q = 0)$, Fig. 6c) decreases with increasing structure height. However, it seems to tend towards a constant value and not to zero. This fact is most probably due to the finite size of the network used in numerical calculations.

The work presented in **[O2]** also involved scanning confocal laser microscopy of the 3-dimensional networks, (Fig. 6a-b). The polymer photoresist showed sufficient autofluorescence, so the use of a dye was not necessary. 3D reconstructions of the hyperuniform networks attest to their high quality.

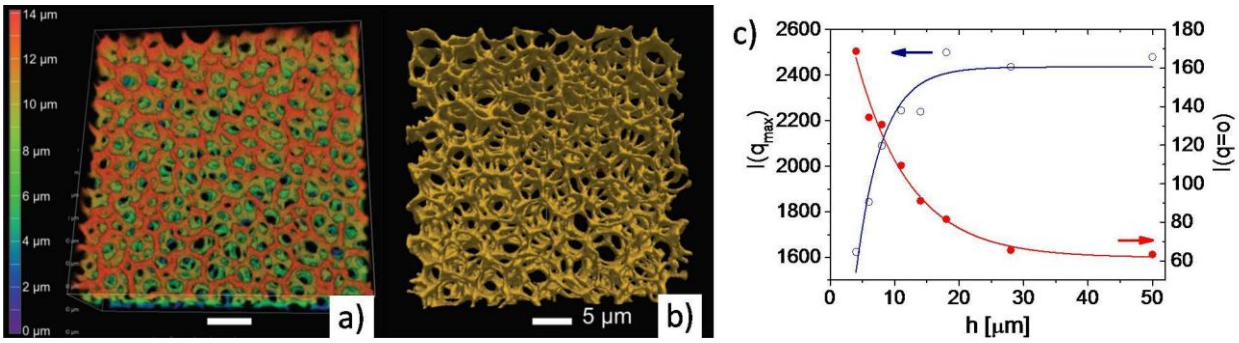

Fig. 6: a-b) Reconstructions of hyperuniform networks based on scanning laser confocal microscopy measurements c) Evolution of the diffraction ring maximum ($I(q_{max})$, blue) and the intensity scattered at short wavevectors ($I(q=0)$, red) as a function of the network height, *h.*

The 3D laser nanolithography possesses several drawbacks, which adversely affect the geometry of the fabricated structures. The first one stems from the shape of the lithographic voxel, the property described above. Due to its asymmetry, lines parallel to the substrate are elongated ellipses in cross-section, while those perpendicular to the substrate (parallel to the laser beam) have a circular cross-section. So the exact shape of each rod is a function of its angle with respect to the substrate. Another difficulty is connected with the drying process after the solvent bath. While drying, the polymer material undergoes a non-uniform shrinkage – the fragments connected to the substrate stay in place, while those closer to the free surface may shrink considerably. This leads to distortions of the whole structure. In the paper **[O2]** I showed, basing on numerical calculations described above, that the influence of this type of imperfection on scattering properties is small. According to these calculations the shrinkage should lead to a shift of the diffraction maximum by approximately 3.9% towards longer wavevectors. In turn in order to assess the influence of voxel elongation I have calculated $I(q)$ for a structure corresponding to an elongated voxel (ellipsoid with an aspect ratio of 2.9, in accord with the DLW apparatus voxel shape) and a spherical one. I noticed that the voxel elongation leads to a slight decrease of the diffraction peak (by ca. 7%), but apart from that the overall pattern remains unchanged. Basing on these findings I concluded that the imperfections of the writing process should not render the observation of the PBG in networks with a higher refractive index impossible and proceeded to further research aimed at fabricating such networks.

4.3.2.4. Hyperuniform networks with a photonic band-gap

The next step towards an isotropic 3-dimensional materials with a PBG was to increase the refractive index of the dielectric rods. As suggested by numerical calculations [Liew], for the full band-gap to open a refractive index of $n > 3$ is necessary, while the available polymer photoresists have $n = 1.52$. Moreover, the filling structure φ, that is the amount of space occupied by the dielectric material, should fall in the range 0.15 – 0.4, which sets the limitations for the minimum and maximum

rod thickness. Both conditions can be fulfilled if a polymer template is covered with a high refractive index material, which was achieved in the article **[O3]**. First, basing on a hyperuniform point pattern with a characteristic length scale a = 2 μm we fabricated via laser nanolithography a polymer network with φ = 0.15. Next the structure was filled with titania by atomic layer deposition (ALD) with the TiO_2 layer thickness of 8 nm. Following that the polymer template was calcined at 480°C in order to remove the organic material. We thus obtained a network composed of almost pure titania with an average rod thickness (average diameter of the cross-section, $\langle D \rangle = \sqrt{a \cdot b}$, where a and b are the long and short axes of the lithographic voxel) of 220 nm. This corresponds to the filling fraction of only 0.04. The fact that such a loose network is sufficiently stable mechanically to support the next fabrication steps is indeed noteworthy. Finally the sample was subjected to a high-temperature (480°C) chemical vapour deposition (CVD) process to infiltrate it with amorphous silicon. As a result we obtained a composite replica of the initial polymer network, built of silicon and titania. The content of the latter compound is estimated at ca. 25% by volume. Basing on my numerical calculations as well as SEM and FIB-SEM measurements we estimate the filling fraction of the inorganic network at $\varphi \approx 0.15$ with an average rod diameter of $\langle D \rangle$ = 418 nm. The average refractive index of the rod dielectric is estimated at 3.3.

In order to measure the optical properties of the networks we performed spectroscopic measurements with a Fourier-transform infrared spectrometer (FTIR). The light in this instrument is incident on the sample through a Cassegrain lens with the incidence angles between 10° and 30° with respect to the normal. An identical lens is used as an objective. Although in the experiment we measure a distribution of wave vectors, this does not considerably influence the spectral characteristics due to isotropic properties of the networks. The measured transmission has a minimum centred at $\lambda \approx 2.6$ μm (Fig. 7b). The intensity in the minimum decreases (the transmission dip becomes more prominent) with increasing the structure height from 6 μm to 9 μm and a further increase in the structure height leads to a fall in transmission above and below the minimum. This is probably caused by the accumulation of defects in higher structures during their complicated, multi-step fabrication process. In order to make sure that the observed minimum is caused by the specific network geometry and not, for instance, light absorption, we carried out several tests. First of all we repeated the whole fabrication process, but this time starting from a non-hyperuniform, random point pattern (albeit with the same number density, that is the number of points per μm^3, as the hyperuniform one). My calculations of scattered intensities $I(q)$ for a hyperuniform and a random network are shown in Figs. 7c and d (cross-section through $I(q)$ at $q_z = 0$). It is evident that these functions are completely different. While the hyperuniform system is characterized by a ring of high intensity, resulting from the short-range order and isotropy, the random network is devoid of this feature. Furthermore, the latter structure after infiltration with TiO_2 and silicon does not possess any photonic band-gap (Fig. 7b, open squares). In the next experiment we tested longer CVD infiltration times, which meant a thicker silicon layer, a higher filling fraction and as a result a higher effective refractive index of the network. As expected, this lead to a red-shift of the minimum (results in **[O3]**, not shown here). This indicates that the underlying reason of the minimum is indeed the photonic band-gap.

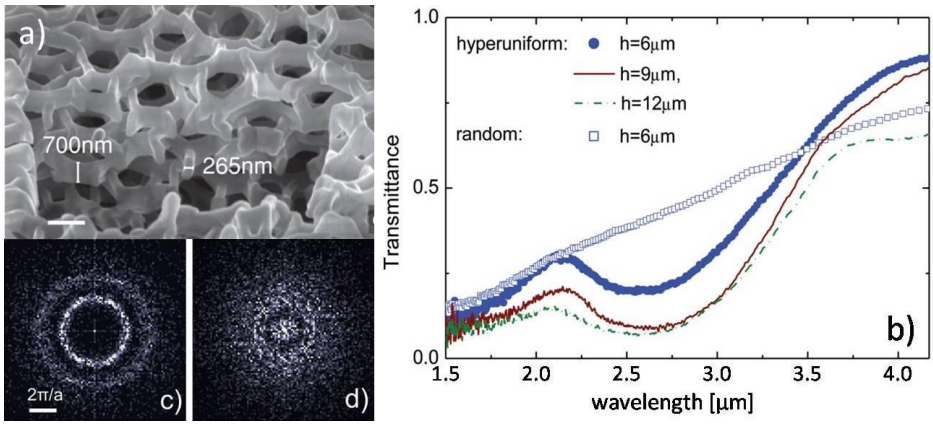

Fig. 7: a) FIB-SEM micrograph of a hyperuniform network with a high refractive index (TiO_2/SI). b) FTIR measurements of light transmission through hyperuniform networks of different heights and a network based on a random point pattern. Cross-section through the scattering function $I(q)$ at $q_z = 0$ for a c) hyperuniform and d) random network.

The method of replicating a polymer network in a inorganic dielectric material described above and in the article **[O3]** has a drawback – the rods are built of a non-uniform material, which reduces their refractive index. Another publication in the series presented here (**0**) shows how to produce a pure silicon replica in a slightly different process. First of all, further optimization allowed for another miniaturization step, we were able to fabricate polymer networks with the characteristic length scale of a = 1.54 μm, which is a 23-percent improvement with respect to the results shown previously. A double inversion process described below was first proposed by Tétreault et al. [Tetr]. In case of our networks the structure is first completely infiltrated with zinc oxide by means of ALD. A surplus of ZnO at the sample surface is etched with argon plasma and the polymer is calcined at 500°C. This results in an inverse structure – an air network in a ZnO matrix. Further on the air voids are filled with amorphous Si in a high-temperature (480°C) CVD process and the ZnO matrix is dissolved with a dilute (10%) HCl. Two more processes are still necessary at this point: heating at 600°C to transform Si from the amorphous to the polycrystalline state and Ar-SF_6 plasma etching to remove excess silicon form the sample surface. FTIR spectroscopic measurements (Fig. 8a) demonstrate a clear minimum in transmission, resulting from a photonic band-gap in the structure.

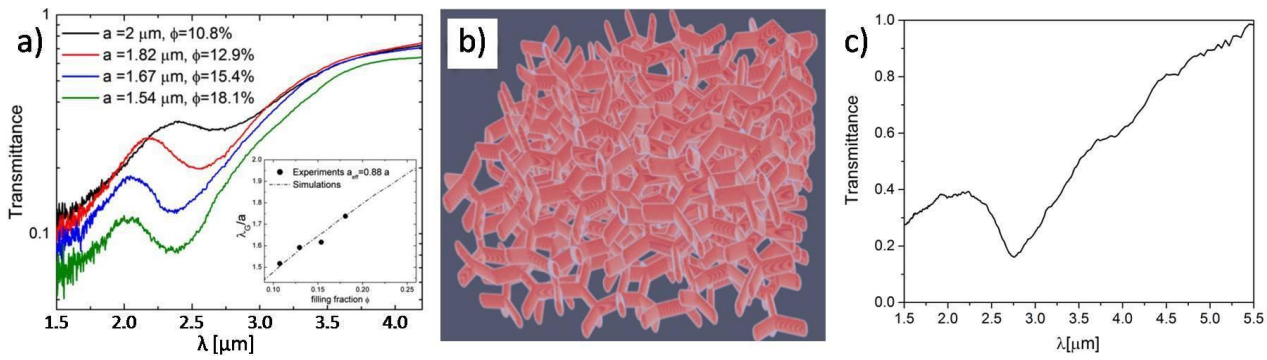

Fig. 8: a) FTIR transmission measurements of hyperuniform networks with different characteristic length scales and filling fractions. b) A computer model of a network, taking into account the lithographic voxel shape, used in FDTD simulations. c) FDTD simulation of light transmission through a hyperuniform network. Network parameters: refractive index 3.1, height 5.5 μm, filling fraction 0.13.

Decreasing the characteristic length scale a (which, as before, is equal to a sphere diameter in the initial RCP point pattern) leads to two effects. First, due to the scaling properties of the Maxwell's

equations, the minimum should blue-shift. Second, decreasing all distances while keeping the thickness of each rod constant increases the filling fraction of the network. This in turn, in contrast to the former effect, should red-shift the transmission spectrum due to the increased effective refractive index. It turns out, however, that the first effect is predominant and, as seen in Fig. 8a, we observe an effective blue-shift of the spectrum.

An effective way of studying light interaction with complicated structures described in this *Summary* is provided by computer simulations. One of the most popular techniques is called Finite Difference Time Domain (FDTD). It depends on solving Maxwell's equations in the time domain on a discrete grid in space and time. Each vertex point of the grid is assigned a value of electric permittivity and magnetic permeability and the Maxwell's equations are discretised. For example a part of Faraday's law of induction (the equation for the *z* component of the magnetic field intensity):

$$\frac{\partial E_y}{\partial x} - \frac{\partial E_x}{\partial y} = -\mu \frac{\partial H_z}{\partial t} \tag{5}$$

in the dicrete form reads:

$$\frac{E_y^n(i+1,j,k) - E_y^n(i,j,k)}{\Delta x} - \frac{E_x^n(i,j+1,k) - E_x^n(i,j,k)}{\Delta y} = -\mu \frac{H_z^{n+1/2}(i,j,k) - H_z^{n-1/2}(i,j,k)}{\Delta t} \tag{6}$$

where *i*, *j*, *k* are indices corresponding to the spatial dimensions *x*, *y* and *z*, *n* is the time index, *Δx* and *Δy* are distances between neighbouring grid points and *Δt* is the time step. This allows to observe the propagation of the electromagnetic field through the analyzed region, calculating frequency-dependent transmission and reflection coefficients or to analyze the polarization state of the transmitted wave. For instance to determine transmission through an object, a light source is set up, typically generating a wave packet covering a certain frequency range *Δf*. Further on, using discretized Maxwell's equations, light propagation is observed and the Poynting vector $\vec{S}$ is determined on a monitor placed behind the object. The integral of $\vec{S}$ over the monitor's surface is equal to the power transmitted through the object and divided by the incoming wave power (determined in a similar way, but for an empty simulation box) yields transmittance. Calculations are performed in the time domain, but during the simulation run the Fourier transforms with respect to time of the $\vec{E}$ and $\vec{H}$ fields is accumulated, for instance for the electric field:

$$\tilde{\vec{E}}(\omega) = \frac{1}{\sqrt{2\pi}} \sum_n e^{i\omega n\Delta t} \vec{E}(n\Delta t)\Delta t \tag{7}$$

This allows to calculate the Poynting vector as a function of frequency $\vec{S}(\omega) = \vec{E}(\omega) \times \vec{H}(\omega)$ and as a result to determine the frequency dependent transmittance in a single simulation run.

In the article **0** I used the MEEP software [Osk], which is an advanced implementation of the FDTD method. I used periodic boundary conditions and a special wave-absorbing material (perfectly-matched layers, PML) on the simulation box borders in the propagation direction. The latter was needed to attenuate the light that passed through the simulated structure. In the computer model of the network I accounted for the lithographic voxel elongation to ensure that the digital representation (Fig. 8b) is as close to the silicon network as possible. The spatial resolution, the number of simulated time steps and other parameters were selected to guarantee convergence with acceptable computational load. Due to numerical complexity, a high demand on memory and the expected long simulation time I decided to

utilise the parallel implementation of MEEP and performed the calculations on a cluster (TeraACMIN, ACMIN, AGH-UST). The simulated photonic band-gap location is in agreement with the experiment for a slightly reduced characteristic length scale $a_{eff} = 0{,}88a$ (Fig. 8a, inset). This shift can easily be explained by a shrinkage of the real network, which could take place at each fabrication step, starting from the drying of the polymer template, through the different stages of double inversion. The shape of the transmission curve (Fig. 8c, here for a slightly lower refractive index $n = 3.1$ than expected for silicon, $n = 3.4$) in the long-wavelength regime and inside the PBG is very similar to the experimental curve. The fact that the measured bandgap appears wider and smoother than the simulated one may be explained by imperfections of the Si network resulting, for example, from inhomogeneous shrinkage and leading to the smearing of the band-gap. Moreover, surface roughness of the rods, which was not taken into account in the simulations, may play a role here. In the shorter wavelength regime the agreement between experiments and simulations is worse. This again may be explained by the surface roughness as well as by the fact that in the experiment only light exiting the sample in a cone of finite opening angle is measured, whereas in the simulations the total transmission is determined.

I would like to mention here that more detailed analyses of light transport through 3D hyperuniform networks were the subject of my further enquiries. An article presenting these new results is currently being prepared and is almost ready for submission (**J. Haberko**, L. S. Froufe-Pérez, F. Scheffold, *Renormalization of diffuse wave transport in three dimensional hyperuniform disordered photonic materials near the band edge*).

4.3.2.5. Hyperuniformity in two dimensions

In the article **[O5]** we focused on two-dimensional hyperuniform systems of two types: i) based on Monte Carlo simulations of hard disks packing (HD) and ii) molecular dynamics simulations with an appropriate potential. In the latter case we obtained the so-called "stealthy" hyperuniform systems (SHU). This property means the structure factor $S(q)$ is equal to zero for wavevectors smaller than a critical value q_c, and not only in the limit $q \to 0$, as in the case of "regular" hyperuniformity. Both types are correlated with each other: while in the SHU structures the structure factor is equal to zero, in the case of HD-derived systems the pair correlation function $g(r)$ is zero for distances smaller than a critical value, since the discs cannot, by definition, intersect. It turns out that despite the differences both systems have similar optical properties and specifically the photonic band-gap width is comparable in both cases. Another reason for our interest in hyperuniform systems without long-range order, apart from their isotropic properties, is potential insensitivity of their optical properties to fabrication defects. In order to verify this assumption we intentionally introduced defects into our simulated networks, which involved cutting randomly chosen network connections. Unfortunately, already a 2.5% addition of defects results in an almost two-fold decrease in the PBG width, both for the HD- and SHU-derived networks. My contribution to this work consisted in providing complementary 3D simulation results, necessary to interpret the results presented in this paper as well as in the data analysis. I estimate my contribution at 10%. Professor Frank Scheffold, who initiated this research, assessed the contributions of all co-authors (with the name order as in point 4.2 of this Summary) at 30/20/10/10/10/10/10%. Consequently, I consider my own contribution to this article to be important and regard this paper as a significant part of the achievement presented here.

4.3.3. Antireflective structures at the tip of the optical fibre

When light is incident on a sharp interface between two media a sudden change in refractive index leads to partial reflection. The reflection coefficient can be calculated from the Fresnel equations and for instance for non-polarized light incident upon an air–glass interface is equal approximately to 4%. In scientific instruments as well as optical devices we use every day such reflections are typically undesirable and we try to avoid them by covering optical elements with antireflective coatings. One can mention here antireflective layers on lenses of eyeglasses, microscope objectives or camera objectives. Typically these layers are based on quarter-wavelength coatings, which lead to destructive interference. This approach works effectively for a narrow distribution of wavelengths. In order to cover a broader range of frequencies costly multi-layer coatings are necessary. An alternative approach is to modify a profile of the interface's refractive index, to smear it out with respect to the step function. The optimal effect is obtained for a quintic function profile shape [Sou]. This, however, leads to another difficulty – the number of materials with different values of the refractive index n is limited, especially in the n range close to unity. But a change in the refractive index profile can also be achieved by modifying the filling fraction of a dielectric material, that is by fabricating small objects at the interface, with characteristic sizes smaller than the wavelength.

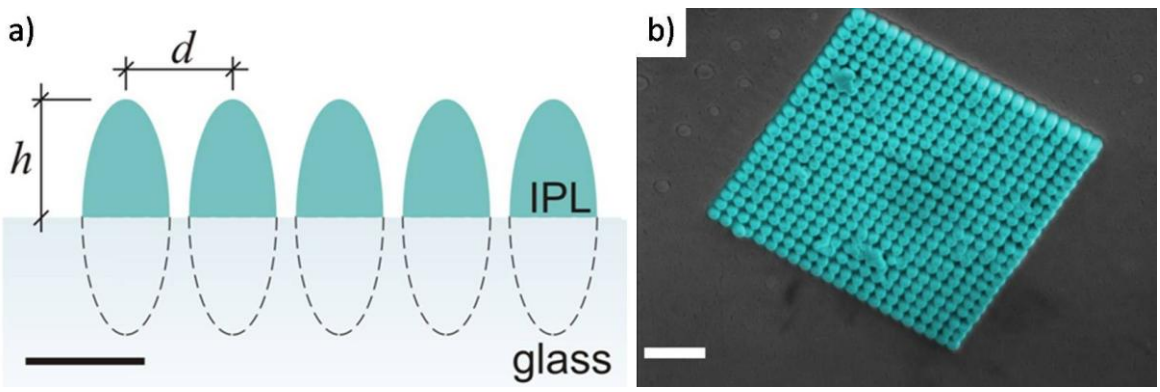

Fig. 9: a) A schematic of an antireflective structure at the optical fibre tip. IPL – polymer photoresist. b) SEM micrographs (false colours) at the optical fibre tip.

The aim of the studies presented in **[O6]** was to reduce the reflection of the infrared wave in a certain wavelength range centred at $\lambda = 1550$ nm (wavelength important in telecommunication) from the optical fibre tip by creating a matrix of small polymer dielectric elements (Fig. 9a) with a non-uniform profile. We used the two-photon laser nanolithography here to write the structures directly at the fibre tip. The distance between the elements should be sub-wavelength to avoid diffraction and in our case is equal to approximately 370 nm. As mentioned above, the lithographic voxel is an elongated ellipse and this is also the shape of the elements in the coating. They are placed on a square grid (Fig. 9b, a false colour SEM image). Such design provided us with two free parameters: the distance between the nearest neighbours (d in Fig. 9a) and the height of an element, h. The former can be changed by programming the movements of the piezoelectric table in the DLW instrument. On the other hand if the laser is focused below the glass substrate surface, only part of the voxel will be polymerized. Hence by properly positioning the focus, one can change h.

The FDTD method allowed me to calculate here the profile of the effective refractive index of the layer. To this end I placed in the simulation box a model of the layer as well as a radiation source and monitored the phase of the wave as a function of distance from the glass substrate (that is from the tip of the fibre).I could thus calculate the optical path length, whose derivative with respect to distance

yields the refractive index profile. The results of these calculations for optimal *d* and *h* parameters are shown in Fig. 9b (red curve). Undulations around $n = 1$ are a computational artefact. The refractive index smoothly changes from 1.0 (air) to 1.5 (glass). Although the curve is not very close to the quintic profile, the antireflective properties of the structure studied here are very good. The measured reflection coefficient drops to 0.12% at $\lambda = 1550$ nm and remains below 0.28% in the range 1500–1600 nm. Interestingly, the performance is of high quality despite the defects apparent in Fig. 9b.

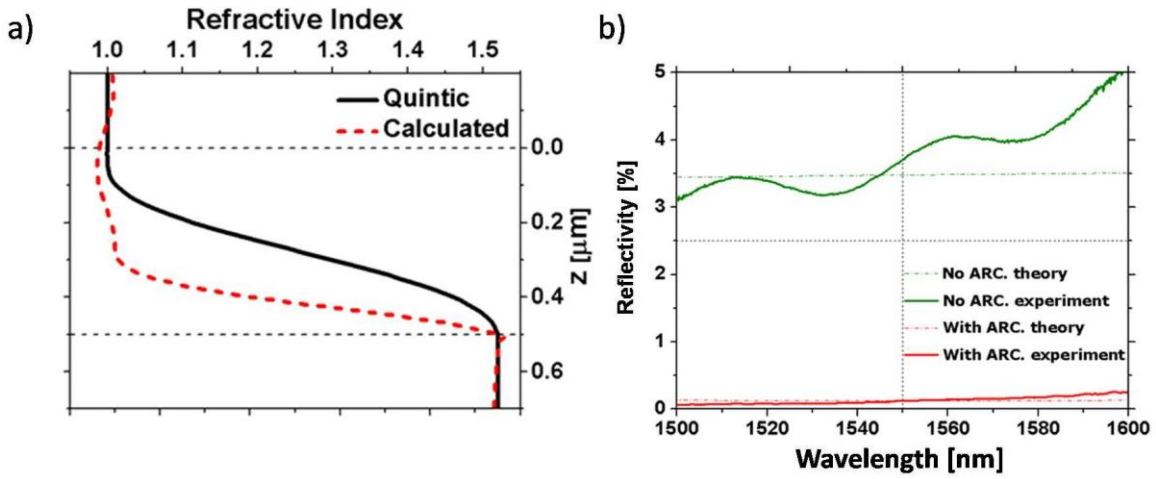

Fig. 10: a) The effective refractive index profile of the antireflective structure as a function of the distance from the glass substrate. Black – a quintic polynomial, red – FDTD simulation results. b) Measured and expected reflectivity from the fibre tip without (green) and with (red) the antireflective coating.

4.3.4. Grating-on-mirror structures with asymmetric transmission

4.3.4.1. Devices with polarization-dependent properties

A metamaterial showing asymmetric transmission is a medium that transmits light incident in one direction, but at the same time reflects waves incident in the opposite direction. In an ideal situation such material would transmit all light travelling in one direction (e.g. from left to right), while completely reflecting the light passing in the opposite direction (from right to left). Research in this field has been carried out for several years. Metamaterials with sub-wavelength metallic elements, such as resonators [Kang] or layers [Li] have been proposed here. Dielectric structures have also been studied, containing a photonic crystal with broken symmetry [Mand]. The article **[O7]**, being part of the achievement presented in this Summary, builds on the idea proposed by Mandatori et al [Mand]; however, a simplification of the design was necessary to enable the fabrication of the metamaterial using available techniques. We show here that manufacturing a metamaterial with asymmetric transmission is feasible and we analyse its transmission curves.

Our metamaterial consists of a Bragg mirror and a diffraction grating on top of it, with a set of parallel lines (Fig. 11a) separated by a distance *d*. The Bragg mirror is a stack built of alternating layers of a high- (n_1) and low-refractive index (n_2) material. Layer thicknesses h_1 and h_2 are equal to:

$$n_1 h_1 = n_2 h_2 = \lambda_o / 4 \tag{8}$$

A mirror of this type is a one-dimensional photonic crystal with a band-gap centred at λ_o for light normally incident on its surface. The band-gap width on the λ scale depends on the dielectric index

contrast. The shape of the transmission curve, in turn, is a function of the number of layers – the more layers, the sharper is the transmittance decrease at the PBG edge.

As I will show below, such material indeed possesses asymmetric transmission. Qualitatively this effect may be explained in the following way. Let us consider a plane wave at normal incidence, travelling in the direction of the Bragg mirror. If the wavelength belongs to the high transmission region (outside the PBG, $\lambda \approx 0.8$ μm in Fig 11d), then almost all photons will pass through. Further on if the wavelength is shorter than the period of the lines ($\lambda < d$) the wave will undergo diffraction. This will not, however, influence the total transmission of the material, which will be high. If, however, the same wave is travelling from the opposite direction, it will first interact with the lines and will be diffracted. A considerable part of the intensity (the exact value will depend on the line geometry) will be directed in the (+/-) first and possibly also higher diffraction orders and this portion of radiation will propagate through the Bragg mirror at a certain angle and not normally as in the previous case. The photonic band-gap position at the wavelength scale for this incidence angle is different, so it may happen that this wave will be reflected. This will result in an effective decrease in the transmitted intensity. It is thus clear that with correctly chosen parameters the total transmission will depend on the incidence direction.

The FDTD method mentioned in the previous sections of this *Summary* is ideal for studying such structure. As part of the studies for article **[O7]** I performed simulations of light propagation through this structure as a function of its parameters: the number of layers in the Bragg mirror, its refractive indices, the geometry of the diffraction grating (thickness, height and distance between the lines and the "filling fraction" of the grating, that is the ratio of line thickness to the distance between lines). I carried out the simulations in two dimensions; due to discrete translational symmetry of the system in the direction perpendicular to the lines I was able to use periodic boundary conditions. I also inserted the PML material inside the box to absorb the wave reflected from the structure. Fig. 11b-c shows a snapshot of the electric field distribution (a certain time after the source with $\lambda = 0.8$ μm and polarized perpendicularly to the lines was switched on) when the wave is first hitting the mirror (b) and for incidence in the opposite direction (c). The distance between lines was equal to 0.951 μm here. Diffraction effects after passing through the grating are clearly visible. Furthermore, the transmitted intensity is higher in the case of the mirror-lines direction (Fig. 11c). Fig. 11d presents the transmission in both directions and the transmission asymmetry (the difference between the two transmissions) as a function of wavelength. All asymmetry vanishes for $\lambda > 0.951$ μm, as for these waves obviously only the zeroth diffraction order is possible and the idea behind the metamaterial does not function any more. For shorter waves the asymmetry is clearly noticeable: the wave travelling in the stack → lines direction ($T_{S=>L}$, black line) interacts with the structure almost in the same way as with the Bragg mirror; however, the transmission curve for the opposite incidence ($T_{L=>S}$, red curve) is considerably different. The asymmetry ($T_{S=>L}$–$T_{L=>S}$) has a maximum at $\lambda = 0.8$ μm and takes on both positive and negative values in the studied range. So these simulations show that the material meets its expectations.

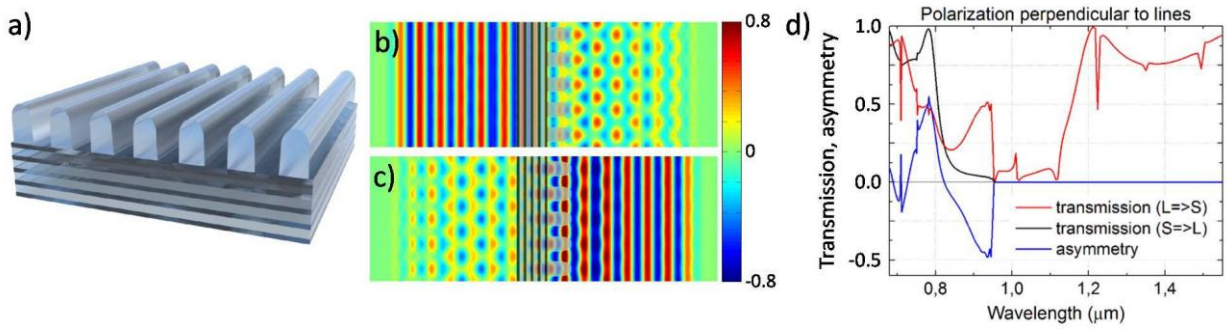

Fig. 11: a) Model of a dielectric grating-on-mirror structure. Electric field intensity (colour scale in arbitrary units) for a λ = 0.8 μm wave polarized perpendicularly to the lines when the wave travels in the b) stack–lines and in the c) lines–stack direction. d) FDTD simulation results of transmission in the two incidence directions and transmission asymmetry.

In the article **[O7]** the FDTD simulations also allowed me to optimize the structural parameters in terms of the highest asymmetry. Fig. 12a shows the results of maximum asymmetry mapping at fixed line distance and the filling fraction (*f*) and line height (*h*) as free parameters. The highest asymmetry was observed for *h* close to 0.9 μm and $f \approx 0.9$. The map also indicates how sensitive the structure is to hypothetical inaccuracies of the fabrication process. In this sense the key parameter is the line height, the filling fraction being less important (a broad region of high asymmetry in Fig. 12a) .

We were able to fabricate the metamaterial described here using a combination of two techniques. The Bragg mirror was manufactured by electron beam evaporation and is made of alternating layers of Nb_2O_5 and SiO_2. The diffraction grating was written on top of the Bragg mirror by direct laser writing. Transmission measurements show a very good qualitative and quantitative agreement with simulation results for light polarized perpendicularly to the lines (Fig. 12b) and the agreement is good in the case of parallel polarization.

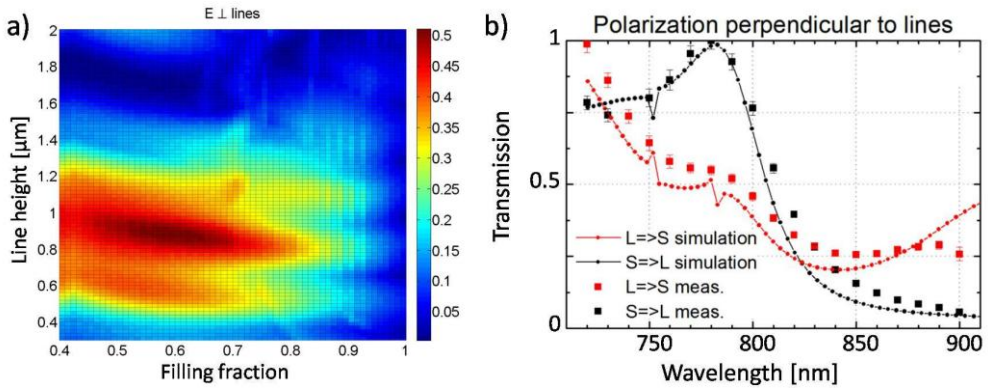

Fig. 12: A map of maximum transmission asymmetry as a function of geometrical parameters of the metamaterials – the filling fraction and the line height b) Comparison of simulated (small symbols) and measured (large symbols) transmission curves for the L→*S* (red) and S→L (black) propagation direction.

4.3.4.2. Asymmetric transmission independent of polarization

Optical properties of the metamaterial described above, and in particular its transmission curves, depend on the polarization of the incident light. The article **[O7]** presents the results for both polarizations, which are different. A natural continuation of these studies was a search for a structure with a similar functionality, but polarization-independent. The outcomes of these trials are described in

a recently published article **0**. The new metamaterial, similarly to the previous one, consists of a Bragg mirror with a diffraction grating fabricated via DLW on top. This time, however, the grating possesses a four-fold rotational symmetry and consists of polymer columns situated on a square grid (Fig. 13a). I simulated the interaction of light with this metamaterial using 3D FDTD simulations. I used periodic boundary conditions and again the absorbing PML material positioned at both ends of the simulation box was responsible for attenuating the wave reflected from and transmitted through the structure. The simulations took into account the exact column shape that can be achieved by the nanolithography and in particular the rounded edges, resulting from the lithographic voxel shape. Thanks to these simulations I was able to identify a region of high asymmetry in the parameter space (Fig. 13b) for the height of columns of approximately 1 µm and their diameter in the range 0.5–0.8 µm. These values were used in the laser writing process. Optical measurements show a very good agreement with simulations (Fig. 13c). The measured asymmetry is slightly lower than the simulated one, which may be due to the shortcomings of the lithographic process. Nevertheless, polarization-independent asymmetry reaching 0.5 was achieved. In order to prove that the structure's properties are indeed independent of polarization, we measured a series of transmission curves, each time rotating the polarization plane with respect to the side of the square field of columns. These asymmetry curves are plotted in Fig. 13c in different shades of green. As expected, the asymmetry remains practically independent of polarization.

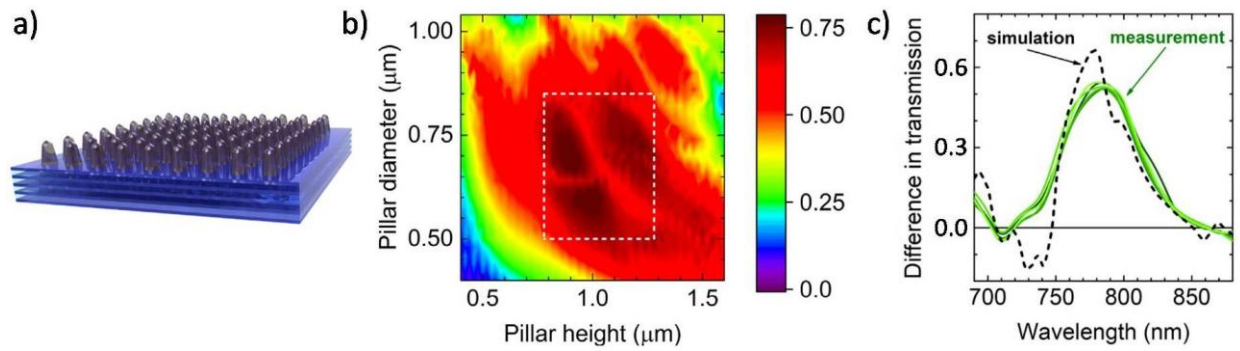

Fig. 13: Model struktury typu "siatka na lustrze" o asymetrycznej transmisji niezależnej od kierunku polaryzacji. b) Optymalizacja parametrów geometrycznych siatki. Mapa maksimum asymetrii w funkcji wysokości kolumn i ich średnicy. c) Różnica w transmisji dla dwóch kierunków propagacji – wynik symulacji (czarna linia przerywana) i eksperymentów (kolory zielone od ciemnego do jasnego odpowiadają polaryzacji skierowanej pod kątem 0^{o}, 15^{o}, 30^{o}, 45^{o}, 90^{o} w stosunku do brzegu struktury z a)).

4.3.5. Matrices of metallic pixels, working as waveplates

The last article being part of the achievement presented here (**[O9]**) describes metallic metamaterials, which could work as waveplates, but in a certain frequency region and not only for one wavelength. The design of this device is presented in Fig. 14a – it consists of a 10x10 matrix of gold cuboids (pixels) with a footprint of 0,4x0,4 μm^2 each and the height that can take up discrete values in the range between 0 and 1.5 µm. I designed a simple stochastic search algorithm, looking for a particular arrangement of pixel heights which would lead to the device working as a half- or a quarter-waveplate. I initialize the algorithm with a random matrix of pixels and carry out a 3D FDTD simulation to check the device's interaction with a linearly-polarized electromagnetic wave. In the next step I calculate the quality factor *F*, which measures how well this particular arrangement of pixels performs as a half- or a quarter-waveplate. To this aim I take into account the ratio of amplitudes r_y/r_x of mutually

perpendicular components of the reflected wave as well as the relative phase shift of these components. Further on I randomly change the height of pixels and re-calculate *F* (basing on a new FDTD simulation run). If the change in height leads to better performance, it is retained and rejected otherwise. This procedure is repeated until the device's characteristics become satisfactory. In order to broaden the searched solution space I run several simulations in parallel, each starting from a different random initial configuration.

My algorithm yielded configurations for which the ratio of amplitudes of mutually perpendicular components was close to unity in a broad wavenumber range (3000 cm^{-1}–4500 cm^{-1}, corresponding to λ =2.2–3.3 μm in vacuum) and their relative phase shift is close to π (half-waveplate) or π/2 (quarter-waveplate). The design protocol described here can easily be expanded to metamaterials modifying the polarization state in a different, more complicated way. It is sufficient to choose *F* properly, in a way defining the quality of the structure in a particular problem.

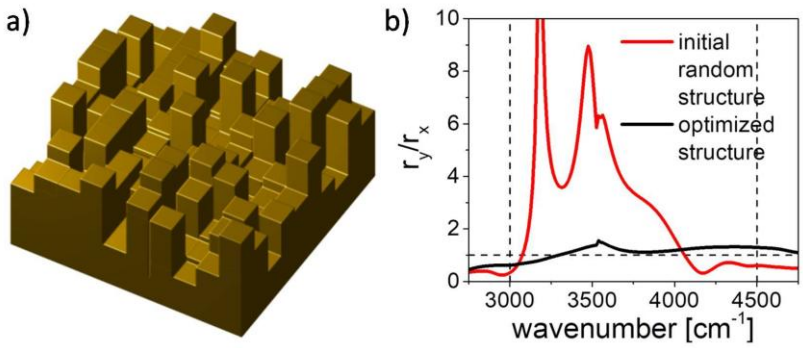

Rys. 14: a) A computer-generated model of a metallic matrix of pixels. b) The ratio of perpendicular components of the wave reflected off the metamaterial – FDTD simulation results.

4.3.6. Synopsis

Optical metamaterials are a fascinating field of physics. Thanks to the rapid progress in microfabrication techniques, such as lithographic methods (with a special emphasis on the laser nanolithography) or techniques based on ion milling (FIB) it is currently possible to fabricate 3D structures with highly complex shapes. This allows to produce materials with interesting, exceptional properties.

In the present Summary I have presented my research concerning several different metamaterials, namely i) non-periodic networks with a short-range order, possessing a photonic band-gap, ii) antireflective coatings for optical fibres, iii) systems with asymmetric light transmission and iv) broadband metallic waveplates. In all cases my contribution to the design, fabrication and characterisation of these systems was substantial. I have managed to generate for the first time 3D hyperuniform polymer networks on the micron scale, which could later be transformed into photonic bandgap materials, which is attested by numerous experimental results (SEM, FIB-SEM, visible light diffraction) – articles **[O1]** and **[O2]**. I have also greatly contributed to obtaining high-refractive index networks with the photonic band-gap (paper **[O3]**, **0**). Furthermore, in designing advanced metamaterials computer simulations are indispensable, as they allow the researcher to predict the material's properties as a function of its geometrical parameters and other characteristics. The FDTD method works particularly well here and I was intensively using this technique while preparing the articles being the basis of the achievement presented here. I used these computations in article **0**, in which they were a vital reference point for experimental results. With my simulations I also contributed

to article **[O5]**, describing two-dimensional hyperuniform networks. In turn, in papers **[O6]–[O9]** the simulations were necessary to design and optimize the metamaterials.

4.3.7. Literature

[Cai] W. Cai, V. Shalaev *Optical metamaterials. Fundamentals and applications,* Springer, 2010

[Yabl] E. Yablonovitch, *Inhibited spontaneous emission in solid-state physics and electronics*, Phys Rev Lett 58 (1987) 2059–2062

[John] S. John, *Localization of photons in certain disordered dielectric superlattices*, Phys. Rev. Lett. 58 (1987) 2486–2489

[Flor1] M. Florescu, S. Torquato, P. J. Steinhardt, *Complete band gaps in two-dimensional photonic quasicrystals*, Phys. Rev. B 80 (2009) 155112

[Flor2] M. Florescu, S. Torquato, P. J. Steinhardt, *Designer disordered materials with large, complete photonic band gaps*, Proc. Natl. Acad. Sci. 106 (2009) 20658-20663

[Liew] S. F. Liew, J.-K. Yang, H. Noh, C. F. Schreck, E. R. Dufresne, C. S. OHern, H. Cao, *Photonic band gaps in three-dimensional network structures with short-range order*, Phys. Rev. A. 84 (2011) 063818

[Man] W. N. Man, M. Florescu, K. Matsuyama, P. Yadak, G. Nahal, S. Hashemizad, E. Williamson, P. Steinhardt, S. Torquato, P. Chaikin, Opt. Express 21 (2013) 19972

[Tetr] N. Tétreault, G. von Freymann, M. Deubel, M. Hermatschweiler, F. Perez-Willard, S. John, M. Wegener, G. A. Ozin, Adv. Mater. 18 (2006) 457

[Osk] A. F. Oskooi, D. Roundy, M. Ibanescu, P. Bermel, J. D. Joannopoulos, S. G. Johnson, *MEEP: a flexible free-software package for electromagnetic simulations by the FDTD method,* Comput. Phys. Commun. 181 (2010) 687

[Sou] W. H. Southwell, *Gradient-index antireflection coatings*, Opt. Lett. 8 (1983) 584

[Kang] M. Kang, J. Chen, H. X. Cui, Y. Li, H. T. Wang, *Asymmetric transmission for linearly polarized electromagnetic radiation*, Opt. Express 19 (2011) 8347

[Li] Z. Li, M. Mutlu, E. Ozbay, *Highly asymmetric transmission of linearly polarized waves realized with a multilayered structure including chiral metamaterials*, J. Phys. D 47 (2014) 075107

[Mand] A. Mandatori, M. Bertolotti, C. Sibilia, *Asymmetric transmission of some two-dimensional photonic* crystals, J. Opt. Soc. Am. B 24 (2007) 685

5. Description of other scientific achievements

Publications described in this section (**[D1]**-**[D18]**) are enumerated in points II.A and II.C of the attached *List of achievements*.

5.1. More about optical metamaterials – matrices of twisted band elements

In the article **[D17]** we managed to create a metamaterial effectively acting as a quarter-wave plate in the wavenumber range of 1100 cm^{-1}–1200 cm^{-1}. The design of this material is however different from the one presented in **[O9]**. It is based on a periodic arrangement of twisted band metallic elements. The

bands are built of rods, parallel to the substrate. My simulations of light interaction with this material show that the ellipticity of the reflected wave indeed remains constant in a certain wavelength range. Furthermore, my simulations showed that the action of the metamaterial is strongly dependent on the twisted bands' height – decreasing it by only 1 μm leads to a completely different polarization state of the reflected wave. We managed to fabricate these structures by laser nanolithography and the polymer templates were then covered with a layer of gold by sputter-coating in vacuum. The experimental results are qualitatively in agreement with the simulations. Some quantitative discrepancies can be explained by the mentioned height sensitivity, especially considering the fact that the absolute height is a parameter that is not well-controlled in the laser nanolithography.

5.2. Thin films of polymer composites

In this application I regard as the most important a series of articles devoted to photonics. I would like to point out, however, that my scientific interests and a considerable part of my publications are related to the physics of thin polymer films and, more generally, organic films, with a special emphasis on their potential applications in organic electronics.

My scientific career started with studies of conjugated polymers. My master thesis addresses the topic of phase separation in thin (~100 nm) films of polymer composites. The first publications were also related to this topic. A sudden interest in electrically conducting polymers started in the 1970s, when high electrical conductivity of doped polyacetylene was discovered. Since that time many other conducting polymers and polymer families were discovered, such as poly(3-alkylthiophenes) (P3ATs) and doped polyaniline (PANI). Their metallic or semi-conducting type of conductivity renders them good candidates for multiple applications in plastic electronics, photovoltaic devices, catalysis and anti-corrosive coatings. Unfortunately, interesting electrical properties of these polymers invariably lead to mechanical properties inferior to those of classical ones. This is due to a system of conjugated π bonds in the macromolecule, which allows for delocalisation of charges along the polymer backbone. A side effect, however, is the increased stiffness of the macromolecule and its partial uncoiling, which affects the molecule's elasticity. One common way to improve mechanical properties of such polymer is to mix it with another, non-conjugated one. However, it often happens that the distance in the solubility parameter space of these two compounds is high, leading to phase separation. Such effect may be undesirable if the processing is aimed at a uniform material, forming an active layer of an electronic device. It is thus important to study the phase separation process in such systems.

In my master thesis I concentrated on thin films of polymer composites containing polyaniline doped with different organic acids (camphorsulfonic acid, CSA and dodecylbenzenesulfonic acid, DBSA, among others). Articles **[D1]** and **[D2]**, published still before obtaining the PhD degree, were devoted to studies of doped polyaniline and polystyrene composites, manufactured by spin-coating (casting a polymer solution onto a rotating substrate). I studied how the humidity and other parameters, such as PANI molar mass or the composition of the spin-coated mixture, influence this process. I found out that the humidity has a profound effect of the film's morphology. Dynamic secondary ion mass spectrometry (dSIMS) measurements showed that in the case of films manufactured in dry atmosphere a layer rich in PANI is formed close to the substrate, while sample preparation in humid atmosphere leads to a more uniform distribution of polymers with respect to depth. Humid atmosphere, in turn, favours the migration of the dopant (CSA in this case) towards the sample's free surface.

I also focused on dendritic structures, growing inside polymer layers in certain conditions; I tried to determine their composition and formation mechanisms. I also successfully tried to direct the phase

separation so as to easily (in one process, that of spin-coating) obtain the desired polymer structures on the substrate. To this aim I modified the substrate with hydrophilic and hydrophobic self-assembled monolayers (SAMs). In the course of studies presented in the paper **[D3]** I managed to produce two types of regions within one sample: with high PANI concentration close to the substrate and with uniform PANI distribution as a function of depth. These regions mimic the size and shape of SAM-modified areas, which was attested by optical microscopy, atomic force microscopy and SIMS measurements. Furthermore, I studied electrical conductivity of thin polymer films (**[D4]**).

Chemical modifications of the substrate by the deposition of SAMs in order to direct the phase separation process, were also a topic of three other articles (published after my PhD), of which I am a co-author (**[D5]**, **[D6]**, **[D18]**).

The above mentioned dendritic structures seemed such an appealing subject to me that I decided to devote more effort to studying them. In the paper **[D7]** I concentrated on dendrites formed in thin-film composites containing PANI and its oligomer analogue (Fig. 14a) as well as conventional (i.e. non-conjugated) polymers: polystyrene (PS) and poly(methyl methacrylate) (PMMA). These studies showed that in the case of PANI-containing layers, the dendrites are built of its conventional companion, that is PS or PMMA. The layer morphology is very interesting and complex here – dendrites are surrounded by a porous conventional polymer layer and the bottom of pores is filled with PANI. In contrast, in films containing PANI's oligomer analogue, dendrites seem to be the oligomer's crystallites. In data analysis computer simulations of diffusion-limited aggregation proved particularly useful (Fig. 14c).

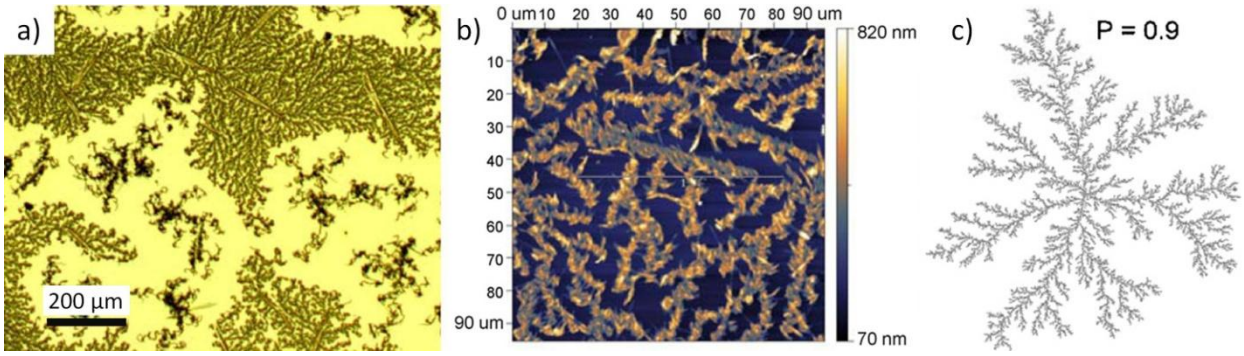

Fig. 14: a) Optical micrograph of dendrites in a thin film containing an oligomer analogue of PANI and polystyrene b) Topography of dendrites measured by atomic force microscopy. c) Computer simulations of diffusion-limited aggregation.

Thin films of PANI composites are generally characterised by interesting morphological structures. It is also true for PANI doped with camphorsulfonic acid. In my article **[D10]** I showed that in this case the dopant has the most significant impact on the sample's morphology. Due to its amphiphilic character it promotes the formation of PANI domains visible on the sample surface.

5.3. X-Ray Photoemission Spectroscopy in studies of organic materials

X-ray photoelectron spectroscopy (XPS) is an important experimental technique in the domain of thin organic films. It can both qualitatively and quantitatively determine surface composition. Moreover, high-resolution XPS instruments are capable of identifying individual chemical states of atoms in the sample. I have published several papers, where XPS provided key information concerning sample's compositions: **[D8]**, **[D12]**-**[D14]** and **[D16]**. The method is not, however, limited to surface studies, although typically the recorded photoelectrons indeed come from a thin layer of 5 nm thickness

close to the sample's free surface. Ion sputtering helps to access deeper regions of the sample. A typical approach to such experiments is to repeat several cycles of XPS measurements followed by sputtering away of the sample's outer layer with a monoatomic ion beam in the keV range. As a consequence one can in principle observe the changes in composition and chemical states as a function of depth. While this methodology works well for inorganic materials, it is not particularly well-suited for organics, including polymers. In this case it leads to considerable chemical damage to the delicate material. Moreover, intensive ballistic mixing of the atoms changes the composition. These problems can be avoided if a beam of large (approximately 2500 atoms) ionised clusters e.g. of a noble gas is used instead (gas cluster ion beam, GCIB). A large projectile deposits most of its kinetic energy close to the sample surface, leaving deeper regions intact. Consequently, the measured XPS spectrum is not disrupted by the effects mentioned above and reflects the true composition of the sample. XPS combined with GCIB sputtering is thus an ideal technique to measure chemical composition depth profiles in organic films.

In the article **[D13]** I used XPS combined with GCIB depth profiling to analyse processes happening in active layers of photodetectors during simulated aging. One of the drawbacks of organic electronics is its sensitivity to humidity, temperature, oxygen and sunlight. Hence aging studies are of utmost importance, as they show whether a particular material has a potential to be used in future devices or if it would degrade under normal conditions. In the course of research summarised in article **[D13]** I studied thin (~250 nm) films of organic mixtures containing PCBM (a derivative of the buckyball fullerene C_{60}, often utilised as electron acceptor in organic photovoltaic devices) and a PBDTTT-C polymer (electron donor, also utilised in organic photovoltaics), deposited on a transparent indium tin oxide (ITO) electrode. The carbon C1s XPS spectrum in this system is quite complicated (Fig. 15a) and it can be decomposed into five peaks, each of which can be attributed to carbon atoms with different coordination. For instance peak no. 1 comes from photoelectrons ejected from C-C carbons in PBDTTT-C and the fullerene part of PCBM, as well as in the benzene ring of PCBM. Peak no. 2 corresponds to C-C-coordinated carbon atoms in the PCBM's side chain and C-O carbons in PBDTTT-C. I studied how the composition of thin films was influenced by two types of simulated aging: i) "light aging" carried out in dry nitrogen atmosphere in the presence of white light and ii) heating (at 65^{o}C) in humid air atmosphere with relative humidity of 85%. GCIB depth profiling shows (Fig. 15b) that all samples (including the non-aged one) are enriched in oxygen close to the free surface (sputtering time = 0). However, in the case of aged samples the degraded, oxygen-rich region stretches deeper below the surface and in the sample aged with light the enrichment is much higher than for a non-aged sample. Intensity measurements of individual peaks as a function of the sputtering time (which is equivalent to the depth below the surface) show that the double C=O bonds may break as a result of irradiation and the combined action of increased temperature and high relative humidity may lead to the migration of PBDTTT-C towards the free surface. Moreover, the latter type of aging may result in partial chemical decomposition of PCBM. I would like to underline that monoatomic ion sputtering would be completely pointless here as it would damage the studied material and make the observation of these subtle XPS effects impossible. So a combination of XPS and GCIB opens entirely new research possibilities in the field of organic thin films and the number of articles using these combined techniques is, to date, still limited.

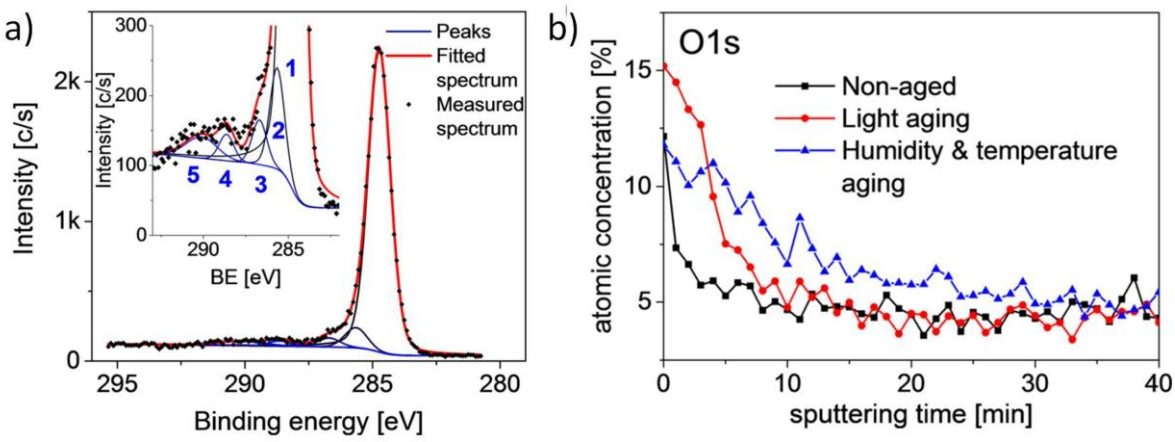

Fig. 15: a) XPS surface spectrum of a PBDTTT-C/PCBM mixture working as an active layer in a photodetector, decomposed into contributions from individual chemical states. b) Oxygen concentration at and below the surface of the non-aged and aged photodetectors.

XPS combined with GCIB sputtering was also intensively used in studies presented in article **[D12]**. We show here that although the ion sputtering process itself does not damage the organic material lying directly below the sputtered layer, a combination of the X-ray and cluster ion beams may lead to the cross-linking or chain scission of polymer backbones. However, in the case of materials studied here (polyalkylthiophenes, polystyrene, poly(methyl methacrylate)), the chemical structure within one repeat unit is retained, unaltered by the sputtering process. This is attested by stable XPS spectra, unchanged by radiation and cluster ions.

The paper **[D14]** is another example showing how much information about organic materials can be obtained from XPS linked with GCIB sputtering. Here we study polymer core-shell microspheres (or spherical colloidal particles) with a sub-micron diameter, synthesised on three slightly different routes. The particles' core is built of polystyrene and the shell consists of a copolymer containing styrene and a polyglycidol derivative. The latter may in turn be viewed as a derivative of poly(ethylene glycol) (PEG). PEG possesses numerous interesting biomedical applications. It is water soluble and can be chemically bonded to active ingredients of drugs, which prolongs their action in the organism, it can also be used to coat medical instruments, which renders them hydrophilic.

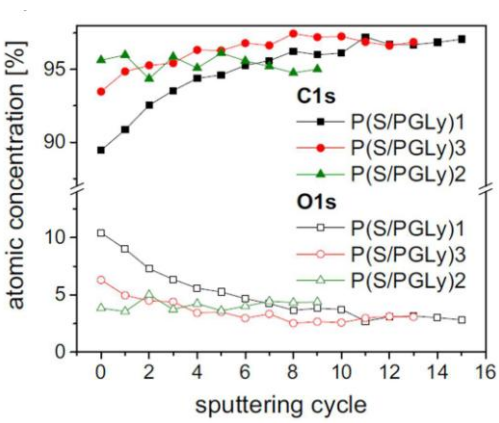

Fig. 16: Atomic concentratiosn of oxegen and carbon inside a microsphere as a function of depth, determined by XPS for different synthetis routes (P(S/PGLy)1–3). These curves prove that by changing the synthetic conditions one can tune the chemical composition profile of the spheres.

So the colloidal particles discussed here could potentially have biomedical applications as well. Thanks to XPS experiments I was able to show that each synthesis route leads to a different distribution of oxygen and hence also of the PGL derivative (oxygen is present only in this compound) as a function of distance from the microsphere centre (Fig. 16). Such measurements effectively allow to design a PGL composition profile inside a microsphere and to manufacture such particles.

The articles **[D8]** and **[D16]** were also devoted to XPS studies of organic materials. In this case, however, I did not use the depth profiling. In **[D8]** XPS was used to study the adhesion of proteins to the substrate. In the paper **[D16]** my XPS measurements proved the effectiveness of grafting polymers on a different polymer substrate and of their chemical modification by electron beam lithography.

5.4. Other publications

The Kelvin Probe Force Microscopy (KPFM) is another effective experimental method that can be applied to thin organic films. It allows to measure, with a resolution typical of atomic force microscopy, the local work function of the sample. It turns out that the contact potential difference, determined during these experiments, is sensitive to dipole moments induced inside the studied thin film and not only at its free surface. It is thus possible, using this technique, to study interfaces inside multilayered samples, such as between the electrode and the active layer of a photovoltaic device. In the article **[D9]** we studied polystyrene films deposited on substrates covered with gold, which was modified with hydrophilic or hydrophobic self-assembled monolayers (SAMs) by means of microcontact printing (Fig. 17a). The dipole moment of SAM molecules alters the contact potential difference to such extent that the pattern at the substrate becomes visible in KPFM, despite being completely covered with a polystyrene layer. In turn in the case of PANI(CSA)/PS mixtures the Kelvin method shows how the PANI(CSA) domains interact with the substrate, which changes the contact potential difference value (Fig. 17b).

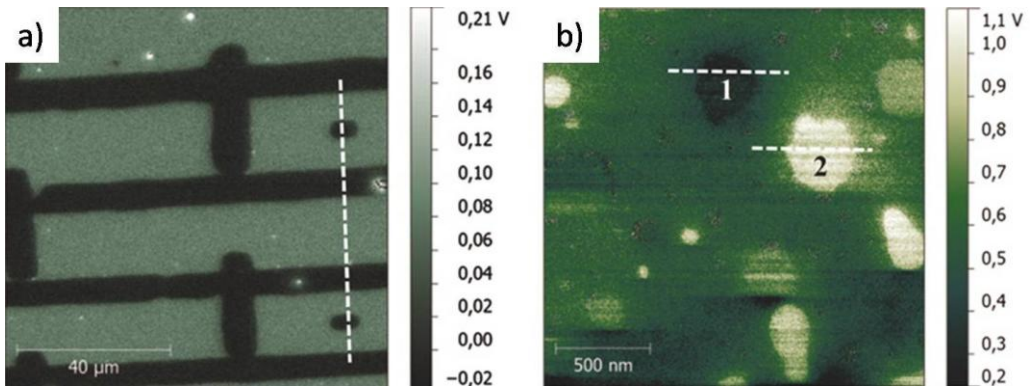

Rys. 17: Kontaktowa różnica potencjału między sondą Kelvina a podłożem. a) Warstwa PS na podłożu Au modyfikowanym wzorem SAM. b) Cienka warstwa domieszkowanej polianiliny i polistyrenu PANI(CSA)/PS.

The studies presented in **[D15]** refer to materials engineering and attest to my broad scientific interests. My contribution to this work consisted in analyzing the results of UV-Vis-NIR spectroscopic measurements and writing several sections of the article. The paper is devoted to the synthesis of polycrystalline zirconia, stabilized with yttria and small amounts (0.5% mol.) of oxides of selected rare-earth elements (ZrO_2-Y_2O_3-RE_2O_3). The material in question in characterised by high hardness and relatively high refractive index (around 2.2 in the visible range), much higher than for instance silica based glasses. Thanks to these features it has found many optical applications. The sintered samples

analysed here are transparent in the near infrared and the visible range, but the total transmission gradually decreases close to the edge of the visible range. The absorption edge is observed at approximately λ = 300 nm, which results from the band-gap in the ZrO_2-Y_2O_3 semiconductor. A small addition of a rare-earth oxide (Gd, Sm or Nd) results in a 20-30 nm shift of the edge towards longer wavelengths, which may be due to structural defects introduced in this process or additional electronic states appearing inside the band-gap. This leads to the band-gap becoming narrower. A relatively high reflection coefficient at the sample surface (~14%) may be explained by the high refractive index of the samples – the agreement between experimental results and the Fresnel equations is very good for all but one sample. In samaria and neodymia-doped samples absorption bands are also visible and their location agrees well with absorption spectra of Nd^{3+} and Sm^{3+} ions available in literature.

Another publication I co-authored, **[D11]**, describes research into mechanical properties of oil-in-water emulsions. In this paper we proposed a model describing the elastic shear modulus and the yield stress of emulsions as a function of their composition (φ, oil content by volume). It must be stressed here that these measurements were experimentally challenging. In the first step the stock emulsion was created by mixing oil and water in the presence of an ionic surfactant (sodium dodecylsulphate, SDS). Further on, intensive processing in a shear cell lead to the breaking of droplets. At this stage the droplets were small (maximum diameter of several μm), but polydisperse. Next the emulsion was fractionated using the depletion interaction induced by SDS micelles. Mechanical properties of thus produced monodisperse emulsions were studied with an oscillatory rheometer. The model proposed here correctly describes the elastic shear modulus and the yield stress for a broad range of droplet diameters (several tens to several hundred nanometers). My input into this work relied on preparing several series of emulsions and performing a considerable part of the rheometric measurements.

6. Description of didactic and organisational achievements

6.1. Didactic achievements

The main part of my teaching duties has been perform at my home institution, AGH University of Science and Technology (AGH-UST). In the last students' survey, which was carried out in 2015, my teaching efforts were highly graded by students – I was awarded the average rating of 4.7 (the scale was 2.0–5.0, the survey was completed by approximately 50 students). I used to teach or have been teaching several subject in the domain of physics and computer science, some of them general, while the others more specialised. As far as physics is concerned these include:

- Exercises in physics for first year students of several faculties at AGH-UST
- Optional exercises in physics for first year students with deficiencies in this domain. The exercises were offered to several faculties at AGH-UST and were organised within the scope of the "Fabryka inżynierów" ("The factory of engineers") programme, financed by the EU Human Capital Operational Programme.
- Exercises "Introduction to quantum and statistical physics", Faculty of Physics and Applied Computer Science, AGH-UST
- Exercises "Introduction to solid state physics", Faculty of Physics and Applied Computer Science, AGH-UST

– Lecture and exercises "Soft matter physics", Faculty of Physics and Applied Computer Science, Faculty of Electrical Engineering, Automatics, Computer Science and Biomedical Engineering, AGH-UST

With respect to computer science I have experience in teaching the following subjects:

– "Genetic algorithms" – computer lab and students' project, Faculty of Physics and Applied Computer Science, AGH-UST
– "Video and animation in computer systems" – computer lab, students' project and seminar, Faculty of Physics and Applied Computer Science, AGH-UST
– "Computer databases" – computer lab, Faculty of Physics and Applied Computer Science, AGH-UST

My teaching duties also involve supervision of diploma theses. I was a supervisor of 10 engineer theses and two master theses, which have already been defended. Currently I supervise four more master theses, which are still under preparation. The titles of these theses can be found in the attached *List of achievements (point III.L)*.

I also regard trainings in experimental and computational techniques, which I organised many times, as an important part of my didactic achievements. Several times I arranged such trainings in atomic force microscopy for PhD students at the Faculty of Physics and Computer Science, AGH-UST. Moreover, since 2013 each year I organise a presentation on X-ray Photoemission Spectroscopy for PhD students of the Faculty of Materials Science and Ceramics, AGH-UST. In November 2013 I was asked to prepare a training on the FDTD method for master and PhD students of the Faculty of Physics at the Warsaw University.

I was also able to continue my teaching during a post-doc stay at Fribourg University in Switzerland. Apart from research work, during four semesters I was involved in teaching students' labs at this university. I used to teach classes of mechanics, optics, rheology and thermodynamics. The classes were in French, English, or German, depending on the students' preferences. Apart from that I informally supervised a master student of the Department of Physics. His thesis entitled *Randomly Generated Defects in FCC Woodpile Photonic Crystals* was defended in Feb. 2012.

6.2. Organisational achievements

Apart from my research and teaching activities I am trying to serve the academic community with organisational efforts.

In 2016 I was elected a member of the **Faculty Council** at the Faculty of Physics and Applied Computer Science as a representative of employees without the habilitation degree.

Since October 2015 I participate in the works of the **University Panel for the Quality of Teaching** (Uczelniany Zespółu d/s Jakości Kształcenia), where I represent the Faculty of Physics and Applied Computer Science. At the beginning I substituted another member and was later on nominated to the Panel for the term 2016-2020. The aim of the Panel is to enhance the quality of teaching at AGH-UST. Our responsibilities involve preparing annual reports pertaining the quality of teaching, elaborating self-assessment report templates for the University's faculties, analysing these reports and preparing their summaries for the University authorities. Panel meetings take place once every month, apart from that extra work is needed to prepare the necessary documents.

I am also a member of the **Faculty Panel for the Quality of Teaching** (Wydziałowy Zespół d/s Jakości Jakości Kształcenia) at the Faculty of Physics and Applied Computer Science. The purpose of this board is to implement the solutions suggested by the University Panel by organising, among other things, surveys for students and employees as well as inspections of selected classes. The panel also provides opinion on some regulation changes of the Faculty Council's commissions. The membership in this panel requires considerable effort, especially at the time the above-mentioned surveys are organised, that is at the end of each semester.

Furthermore, in 2016 I was nominated by the University authorities to the Council of the **S. Staszic Stipend Fund**, operating at the University. Our goal is to award social and educational stipends to AGH-UST students coming from East and Central European countries as well as the developing countries. The council establishes rules according to which the stipends are awarded and prepares a ranking of names, which is then presented to the Rector.

I am also responsible for the web page of the Department of Condensed Matter Physics at my faculty.

7. List of published scientific articles not being part of the achievement specified in point 4.

For details concerning my individual contribution to each of these articles and the journals' impact factors please cf. the attached *List of achievements*, point II.A. and II.C

Before obtaining the PhD degree

[D1] **J. Haberko**, A. Bernasik, J. Włodarczyk-Miśkiewicz, W. Łużny, J. Raczkowska, J. Rysz, A. Budkowski, *The structure of thin films of polyaniline/polystyrene polymer blends studied by SIMS*, Fibres & Textiles in Eastern Europe 13, 103–106 (2005).

[D2] A. Bernasik, **J. Haberko**, J. Włodarczyk-Miśkiewicz, J. Raczkowska, W. Łużny, A. Budkowski, K. Kowalski, J. Rysz, *Influence of humid atmosphere on phase separation in polyaniline-polystyrene thin films*, Synthetic Metals 155, 516–522 (2005).

[D3] **J. Haberko**, J. Raczkowska, A. Bernasik, J. Rysz, A. Budkowski, W. Łużny, *Pattern replication in polyaniline-polystyrene thin films*, Synthetic Metals 157, 935–939 (2007).

[D4] **J. Haberko**, J. Raczkowska, A. Bernasik, J. Rysz, M. Nocuń, J. Nizioł, W. Łużny, A. Budkowski *Conductivity of thin polymer films containing polyaniline*, Molecular Crystals and Liquid Crystals 485, 796–803 (2008).

After obtaining the PhD degree

[D5] A. Budkowski, A. Bernasik, E. Moons, M. Lekka, J. Zemła, J. Jaczewska, **J. Haberko**, J. Raczkowska, J. Rysz, K. Awsiuk *Structures in multicomponent polymer films: their formation, observation and applications in electronics and biotechnology*, Acta Physica Polonica A 115 (2), 435–440 (2009).

[D6] Justyna Jaczewska, Andrzej Budkowski, Andrzej Bernasik, **Jakub Haberko**, Jakub Rysz *Ordering domains of spin cast blends of conjugated and dielectric polymers on surfaces patterned by soft- and photo-lithography*, Soft Matter 5, 234–241 (2009).

[D7] **J. Haberko**, A. Bernasik, W. Łużny, J. Raczkowska, J. Rysz, A. Budkowki *Dendrites and pillars in spin cast blends of polyaniline or its oligomeric analogue*, Synthetic Metals 160 (23–24), 2459–2466 (2010).

[D8] K. Awsiuk, A. Bernasik, M. Kitsara, A. Budkowski, J. Rysz, **J. Haberko**, P. Petrou, K. Beltsios, J. Raczkowska *Protein Coverage on silicon surfaces modified with amino-organic films: a study by AFM and angle-resolved XPS*, Colloids and Surfaces B 80 (1), 63–71 (2010).

[D9] M. M. Marzec, K. Awsiuk, A. Bernasik, J. Rysz, **J. Haberko**, W. Łużny, A. Budkowski *Buried polymer/metal interfaces examined with Kelvin Probe Force Microscopy*, Thin Solid Films 531, 271–276 (2013).

[D10] **Jakub Haberko**, Andrzej Bernasik, Wojciech Łużny, Magdalena Hasik, Joanna Raczkowska, Jakub Rysz, Andrzej Budkowski *Humidity and wetting effects in spin-cast blends of insulating polymers and conducting polyaniline doped with DBSA*, Journal of Applied Polymer Science 127 (3) 2354–2361 (2013).

[D11] Frank Scheffold, James N. Wilking, **Jakub Haberko**, Frédéric Cardinaux, Thomas G. Mason *The jamming elasticity of emulsions stabilized by ionic surfactants*, Soft Matter 10(28) 5040–5044 (2014).

[D12] Andrzej Bernasik, **Jakub Haberko**, Mateusz M. Marzec, Jakub Rysz, Wojciech ŁUŻNY, Andrzej Budkowski *Chemical stability of polymers under argon gas cluster ion beam and x-ray irradiation*, Journal of Vacuum Science & Technology B 34 (3), 030604-1–030604-5 (2016).

[D13] **Jakub Haberko**, Mateusz M. Marzec, Andrzej Bernasik, Wojciech Łużny, Pierre Lienhard, Alexandre Pereira, Jérôme Faure-Vincent, David Djurado, Amélie Revaux *XPS depth profiling of organic photodetectors with the gas cluster ion beam,* Journal of Vacuum Science & Technology B 34 (3), 03H119-1–03H119-5 (2016).

[D14] Monika Gosecka, Joanna Raczkowska, **Jakub Haberko**, Kamil Awsiuk, Jakub Rysz, Andrzej Budkowski, Mateusz M. Marzec, Andrzej Bernasik, Teresa Basinska *Multilayers of poly(styrene/α-tert-butoxy-ω-vinylbenzyl-polyglycidol) microspheres with core-shell morphology: Characterization by AFM, SIMS and XPS*, Colloids and Surfaces A 507, 200–209 (2016).

[D15] **Jakub Haberko**, Anita Trenczek-Zając, Dariusz Zientara, Anna Adamczyk, Krzysztof Haberko, Mirosław M. Bućko *Optical properties of zirconia doped with yttria and some rare earth oxides*, Optical Materials 60, 132–136 (2016).

[D16] Katarzyna Gajos, Vitaliy A. Guzenko, Matthias Dübner, **Jakub Haberko**, Andrzej Budkowski, Celestino Padeste *Electron-Beam Lithographic Grafting of Functional Polymer Structures from Fluoropolymer Substrates*, Langmuir, 32 (41), 10641–10650 (2016).

[D17] Michal Nawrot, **Jakub Haberko**, Łukasz Zinkiewicz, Piotr Wasylczyk *Light polarization management via reflection from arrays of sub-wavelength metallic twisted bands*, Applied Physics B 123, 285 (2017).

Not in the JCR database, published before obtaining the PhD degree

[D18] **Jakub Haberko**, Joanna Raczkowska, Andrzej Bernasik, Wojciech Łużny, Jakub Rysz, Andrzej Budkowski *Pattern formation in thin polymer films containing conducting polyaniline*, Macromolecular Symposia 263 (1), 47–52 (2008).

Jakub Haberko

TABLE OF CONTENTS